# Phases and phase stabilities of $Fe_3X$ alloys ($X$=Al, As, Ge, In, Sb, Si, Sn, Zn) prepared by mechanical alloying

C. Bansal, Z. Q. Gao, L. B. Hong, and B. Fultz
*Division of Engineering and Applied Science, California Institute of Technology, 138-78, Pasadena, California 91125*

(Received 6 June 1994, accepted for publication 1 August 1994)

Mechanical alloying with a Spex 8000 mixer/mill was used to prepare several alloys of the $Fe_3X$ composition, where the solutes $X$ were from groups IIB, IIIB, IVB, and VB of the periodic table. Using x-ray diffractometry and Mössbauer spectrometry, we determined the steady-state phases after milling for long times. The tendencies of the alloys to form the bcc phase after milling are predicted well with the modified usage of a Darken–Gurry plot of electronegativity versus metallic radius. Thermal stabilities of some of these phases were studied. In the cases of $Fe_3Ge$ and $Fe_3Sn$, there was the formation of transient $D0_3$ and $B2$ order during annealing, although this ordered structure was replaced by equilibrium phases upon further annealing.

## I. INTRODUCTION

It is well established that high-energy ball milling can be used to synthesize alloy phases with extended solid solubilities. References 1–12, for example, include reports of extended solid solubilities, although solubility was not always the main topic of study. A systematic study of extended solid solubility promoted by mechanical alloying is best performed with similar solutes under identical experimental conditions. We report here such a study of extended solubility in bcc Fe of the main group solutes Al, As, Ge, In, Sb, Si, Sn, and Zn. X-ray diffractometry was our main technique for determining if the as-milled alloys were bcc, ordered bcc, or if they comprised a mixture of equilibrium compounds. Mössbauer spectrectometry was useful for obtaining information on local chemistry and short-range order in the bcc phase.

There has been recent interest in transient phase formation during the thermal annealing of nonequilibrium alloys. When the transient states occur far from thermodynamic equilibrium, transient state formation must be best understood by kinetic, rather than thermodynamic, arguments.[13–15] In cases where the equilibrium phases form by nucleation and growth, however, thermodynamic explanations with an assumption of suppressed nucleation may be appropriate.[16–18] We have been studying experimentally the kinetic transients in ordered phases,[19] including powders prepared by mechanical alloying.[20] Here we report new observations on transient order in $Fe_3Ge$ and $Fe_3Sn$. We interpret the transient states of $D0_3$ and $B2$ order as an expedient mechanism to reduce free energy before the formation of the equilibrium phases.

We show that the systematics of the as-milled phases can be explained with the first two Hume-Rothery rules.[21–23] We implement these two rules with a Darken–Gurry plot of electronegativity versus metallic radius.[23,24] Mechanical alloying extends the compositional range of bcc solid solubility from the typical 5% for alloys in thermodynamic equilibrium, to 25% in the as-milled alloys of the present study. The transient ordered phase found in annealed $Fe_3Ge$ was much more stable than that in $Fe_3Sn$, perhaps because of the better match of the metallic radii between Fe and Ge.

## II. EXPERIMENT

Alloys of Fe-25 at. % $X$, where $X$=Al, As, Ge, In, Sb, Si, Sn, Zn were prepared by mechanical alloying in a Spex 8000 mixer/mill using elemental powders of 99.9+% purity. Several other alloys of lower composition were also prepared. The powders were sealed under an argon atmosphere in steel vials with ball-to-powder weight ratios of 5:1, and milled for various times. For most alloys we confirmed that 24–36 h of milling time was more than sufficient to achieve a steady-state microstructure. Chemical compositions and micrometer-scale chemical homogeneities were checked using a JEOL Superprobe 733 electron microprobe. Iron contamination from the milling media was significant only for the $Fe_3Si$ alloys, which gained about 2% Fe. Heat treatments were performed with the powders sealed in evacuated glass ampoules. The $Fe_3Sn$ alloy was annealed at 250, 300, 350, 400, and 500 °C for different periods of time whereas the $Fe_{80}Sn_{20}$ and $Fe_{85}Sn_{15}$ alloys were heated at 300 and 400 °C, respectively.

X-ray-diffraction patterns were obtained with an Inel CPS-120 diffractometer using Co $K\alpha$ radiation. Mössbauer spectra were recorded in transmission geometry using a 50 mCi $^{57}Co$ in Rh radiation source. Model-independent hyperfine magnetic-field (HMF) distributions were obtained from the Mössbauer spectra using the method of Le Caër and Dubois.[25] A linear correlation between the values of HMF ($H$) and isomer shift ($I$) was assumed in the form: $I=AH+B$.

## III. RESULTS

X-ray-diffraction patterns from the as-milled alloys prepared in this work are presented in Fig. 1. The as-milled alloys of $Fe_3Al$, $Fe_3Ge$, $Fe_3Si$, and $Fe_3Zn$ were almost entirely the bcc phase. The alloys of $Fe_3As$ and $Fe_3Sb$ contained some bcc phase, although with the presence of a second phase we cannot be sure that the stoichiometry of the bcc phase was $Fe_3X$. We note also that bcc Fe-Zn alloys were

 0021-8979/94/76(10)/5961/6/$6.00  

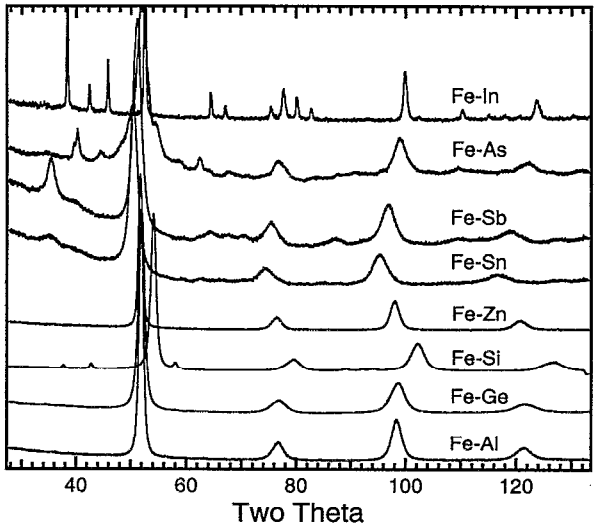


FIG. 1. X-ray-diffraction patterns from as-milled powders of Fe-$X$ powders mixed in 3:1 stoichiometry. Milling time in the Spex mill was 24 h, except for Fe-Ge (16 h) and Fe-As (50 h). The Fe-Si powders were milled in tungsten carbide vials, so small peaks from the milling media are seen.

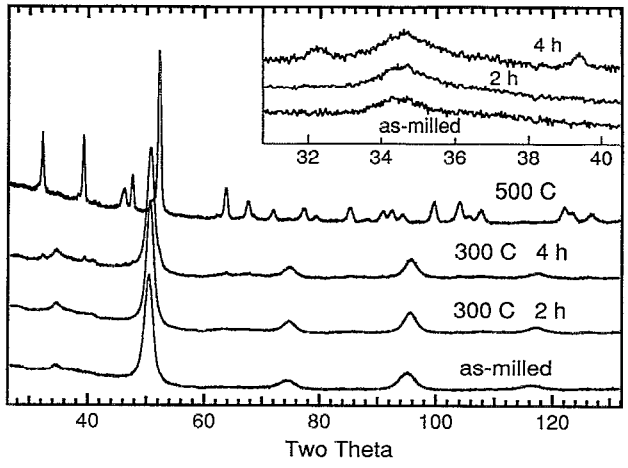


FIG. 2. X-ray-diffraction patterns from $Fe_3Sn$ powder in as-milled state, and after annealing at 300 °C for 2 h, after annealing at 300 °C for 4 h, and after annealing at 500 °C for 5 h. Inset is an enlargement of the region near the (100) superlattice diffraction of the three lower diffraction patterns.

reported previously for alloys prepared by sputtering[26] and cathodic pulverization,[27] and these authors report some tendency for Zn clustering in more concentrated alloys. (Our HMF distributions from the bcc phases in Fe-Zn alloys were narrower than we would have expected from a stoichiometry of $Fe_3X$, perhaps indicating heterogeneities in solute concentration.)

Table I presents results from the analysis of x-ray-diffraction peaks from the bcc phases. The lattice parameters were obtained by the Nelson–Riley extrapolation method[28] with the (110), (200), (211), and (220) diffractions. The grain sizes in Table I were obtained by a Scherrer analysis of the (110) diffraction peaks. Graphs were prepared of the diffraction peak widths in $k$ space to the $k$ vectors of the (110), (200), (211), and (220) diffractions, and the mean-squared strains were obtained from a least-squares fit to the slope of these four points.[29]

In as-milled $Fe_3As$ and $Fe_3Sb$, the $B8$ (NiAs) intermetallic phase was abundant along with the bcc phase. In spite of our best efforts, the Fe-In powders did not form an alloy. Although there were problems with adhesion of In to the walls of the vial, the experimental configuration should have allowed for some alloying of the Fe and In powders. We also milled Fe-In with surfactants such as hexane, but again no alloy was formed. We note that Fe-Sb alloys prepared by sputtering were found to be amorphous.[30,31]

TABLE I. X-ray measurements on the bcc phase of as-milled powders.

| Alloy | Lattice constant (nm) | Grain size (nm) | Strain |
|---|---|---|---|
| $Fe_3Al$ | 0.291 | 11.7 | 0.70% |
| $Fe_3As$ | 0.290 | 8.4 | 1.02% |
| $Fe_3Sb$ | 0.295 | 6.0 | 0.80% |
| $Fe_3Sn$ | 0.298 | 6.0 | 0.78% |
| $Fe_3Zn$ | 0.292 | 13.3 | 0.62% |
| $Fe_3Si$ | 0.285 | 9.6 | 1.10% |
| $Fe_3Ge$ | 0.290 | 8.4 | 1.10% |

Figure 2 shows x-ray-diffraction patterns for $Fe_3Sn$ in the as-milled condition, and after annealing. A bcc phase is not the equilibrium phase according to the phase diagram,[32] which shows a two-phase region below 600 °C and a hexagonal phase intermetallic compound at higher temperatures (750–880 °C). Nasu *et al.*[33] used Mössbauer spectrometry to infer the formation of a bcc Fe-Sn solid solution by mechanical alloying. The presence of $B2$ order has been reported in splat-quenched $Fe_3Sn$.[34]

Besides the fundamental diffractions of the disordered bcc phase, the x-ray-diffraction pattern of $Fe_3Sn$ had a (100) superlattice diffraction characteristic of $B2$ order at $2\theta=35°$. We were concerned that this diffraction could have originated from an intermetallic phase, however. The hexagonal $B8$ (NiAs) structure is such a candidate, although with increasing transition-metal concentration this structure goes continuously to the $B8_2$ ($Ni_2In$ type).[21] The $\gamma$ phase of composition $Fe_{13}Sn_{10}$ has this $B8_2$ structure.[35] In the present work we used mechanical alloying to prepare an alloy of $Fe_{13}Sn_{10}$ stoichiometry, and we found a $B8_2$ ($Ni_2In$ type) structure for the as-milled alloy. Although the (101) diffraction for the $B8_2$ structure coincides with the (100) reflection of the $B2$ structure, other diffractions of the $B8_2$ structure were not observed in the as-milled $Fe_3Sn$. We are confident that the observed diffraction pattern of the as-milled $Fe_3Sn$ indicated $B2$ order in the alloy. As-milled $Fe_{80}Sn_{20}$ and $Fe_{85}Sn_{15}$ also had diffraction patterns characteristic of a $B2$ structure, but their (100) diffractions were weaker. We also believe that there is some $B2$ order in the bcc phase of the as-milled Fe-Sb alloy, since the peak at $2\theta=35°$ is so much stronger than expected from the $B8$ phase alone.

The amount of $B2$ order increased upon annealing at low temperatures, as shown in the inset of Fig. 2. The intensity of the (100) superlattice peak increases from 3.9% of the fundamental (110) peak for the as-milled sample, to 6.5%

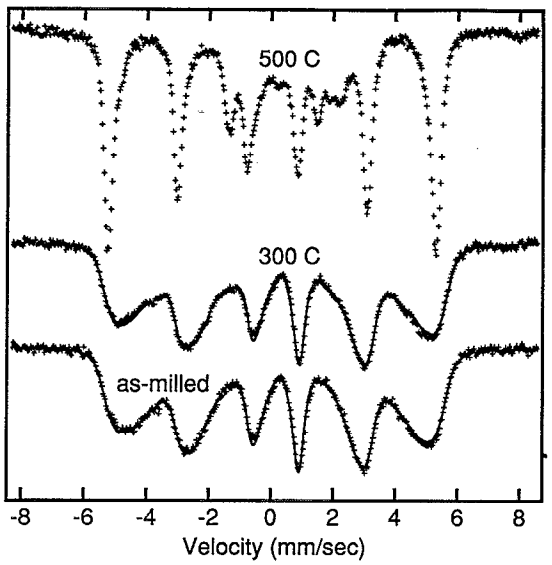


FIG. 3. Mössbauer spectra from $Fe_3Sn$ powder in the as-milled state, and after annealing at 300 °C for 4 h, and after annealing at 500 °C for 5 h.

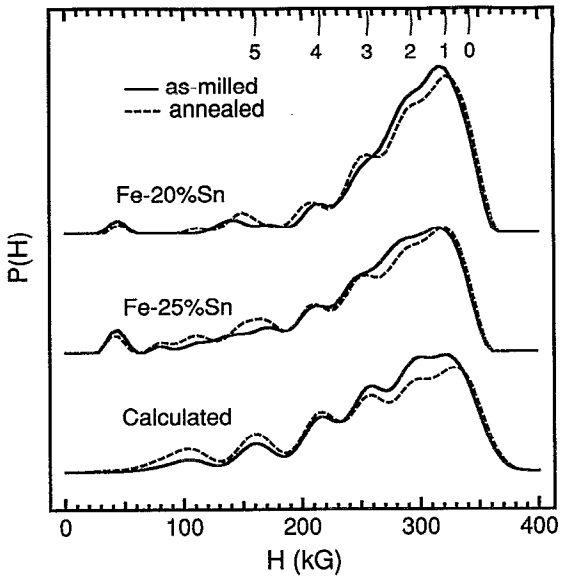


FIG. 4. Hyperfine magnetic-field distributions [probability, $P(H)$, of HMF, $H$]. Top two pairs of distributions are from experimental data such as shown in Fig. 2. Top pair is from $Fe_{75}Sn_{25}$ alloy in its as-milled state (full line), and after annealing at 300 °C for 4 h (dashed line). Middle distribution is from $Fe_{80}Sn_{20}$ alloy in as milled state (solid line) and after annealing at 300 °C for 20 h (dashed line). Lower pair of distributions were calculated as described in the text for states of partial $B2$ order determined from x-ray diffractometry: $L=0.36$ (full line) and $L=0.49$ (dashed line).

after annealing at 300 °C for 2 h. By calculating the intensities of (100) superlattice diffractions for various degrees of order in the $Fe_3Sn$ (including multiplicity, Lorentz-polarization, and form-factor corrections[36]), we found this change corresponded to an increase in the Bragg–Williams LRO parameter $L$ from 0.35 to nearly 0.50 (where 0.50 is the highest possible degree of order for the $Fe_3Sn$ stoichiometry). Upon further annealing there is the growth of the equilibrium hexagonal $B35$ FeSn phase plus bcc $\alpha$-Fe, as seen by the new diffraction peaks from the sample annealed for 4 h. The diffraction pattern for a sample annealed at 500 °C for 5 h (Fig. 2) shows the final phase separation into $\alpha$-Fe and $B35$ FeSn, consistent with the phase diagram.[32]

The presence of $B2$ order in the as-milled material, and its increase upon annealing, was also confirmed by measurements of Mössbauer spectra and HMF distributions (Figs. 3 and 4). A nonmagnetic solute atom such as Sn will reduce the HMF at a neighboring $^{57}Fe$ atom, and the HMF distribution can be used to obtain the distribution of solute neighbors about $^{57}Fe$ atoms.[37] Such assignments of peaks in the HMF distribution to $^{57}Fe$ atoms with different numbers of first-neighbor solute atoms were shown to be very similar for the alloys $Fe_3Al$, $Fe_3Si$, $Fe_3Ge$, and $Fe_3Ga$.[38] We make similar assignments here for $Fe_3Sn$, since the $^{57}Fe$ HMF perturbations caused by Sn neighbors are expected to be like those of other nonmagnetic solutes.[37] Our assignments are shown as numbers at the top of Fig. 4. To help check these assignments, and to interpret the changes in these solute neighborhoods upon $B2$ ordering, a Monte Carlo simulation was performed. These simulations of ordering with a vacancy mechanism were described in detail previously,[14,15,39] and we used the same software for simulating ordering in an $AB_3$ alloy of 65 536 atoms with first-neighbor pair potentials of $V_{AA}=V_{BB}=1.5\ kT$ and $V_{AB}=0$. As order evolved in the simulated alloy, we determined the LRO parameter by integrating the intensity in a cubical volume of edge length $\pi/a$ centered around the (100) diffraction peak.[15] For simulated alloys having values of $L=0.36$ and 0.49, we determined the distribution of the number of $A$ atoms in the first-nearest-neighbor shell of the $B$ atoms by finding all $B$ atoms and counting their neighbors. Simulated HMF distributions were then obtained by superposing Gaussian functions centered at the HMFs determined experimentally for each of the nine possible nearest-neighbor configurations ($B$ atoms with 0–8 $A$ neighbors), but with amplitudes determined from these computed nearest-neighbor distributions. These simulated HMF distributions are presented as the lower pair of curves in Fig. 4. They should correspond approximately to the top two pairs of curves in Fig. 4, which are the experimentally determined HMF distributions for $Fe_{75}Sn_{25}$ and $Fe_{80}Sn_{20}$ as milled, and after annealing at 300 °C for 2 h. There is good qualitative agreement between the simulated and experimental HMF distributions. In both the simulated and the experimental HMF distributions, the probabilities of Fe atoms having 1 or 2 solute neighbors decrease upon $B2$ ordering, whereas the probabilities increase for Fe atoms having 4, 5, or 6 solute neighbors. We tried to perform a more detailed analysis in which we assumed that the Sn concentration in the alloy was inhomogeneous with Sn-rich and Sn-poor regions in the bcc phase. These assumptions did improve the agreement between the calculated and the experimental HMF distributions, but we are not confident that the systematics of the HMF distributions in concentrated Fe-Sn alloys are sufficiently well understood to justify such detailed interpretations.

The as-milled $Fe_3Ge$ was single phase bcc. Upon annealing at 350 °C, there was the formation of transient $D0_3$ or-

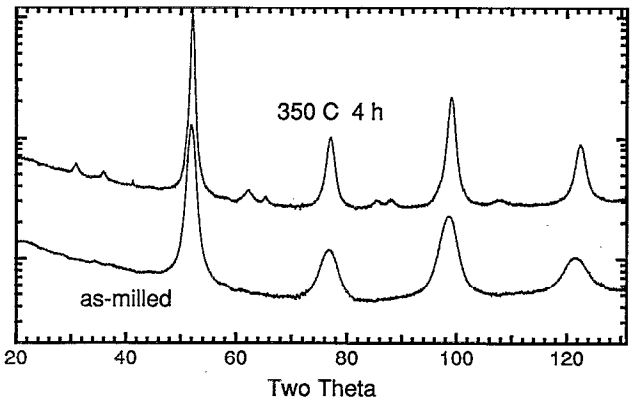


FIG. 5. X-ray-diffraction patterns from $Fe_3Ge$ alloys as-milled for 24 h, and after the milled powder was annealed for 4 h at 350 °C.

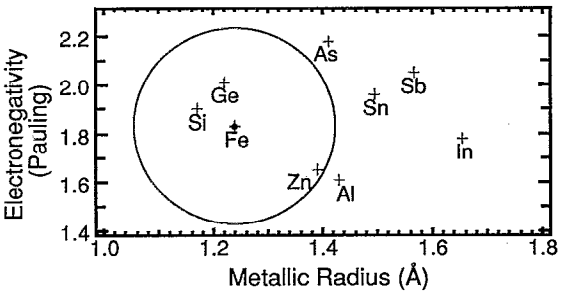


FIG. 7. Darken–Gurry plot for various solutes in Fe. Ellipse was drawn around Fe with a range in electronegativity of ±0.4, and a range of ±15% in metallic radius.

der. This is seen clearly in the x-ray-diffraction patterns presented in Fig. 5, where the formation of the superlattice peaks of the (100) and (1/2 1/2 1/2) families indicate that a high degree of $D0_3$ order had formed after annealing. There was no formation of the equilibrium phases in this material after annealing at 350 °C for 4 h or 300 °C for 24 h, although annealing at 500 °C for 1 h did lead to the formation of the equilibrium phases. Mössbauer spectra of the annealed $Fe_3Ge$ were consistent with the evolution of chemical environments characteristic of the $D0_3$ structure, as reported previously for sputtered films of bcc $Fe_3Ge$.[40] These data, which were obtained at a variety of annealing temperatures,[41] will be reported elsewhere.

## IV. DISCUSSION

### A. Extended solid solubility

The most important Hume–Rothery rule for solid solubility is the size factor rule,[22] which states that good solubility (5 at. % at modest temperatures) requires that the metallic radii of the solute atom and matrix atom differ by less than 15%. Figure 6 shows the metallic radii[21,42] of the solutes in the present study. Approximate boundaries are drawn to show the phases of our as-milled $Fe_3X$ alloys. These phases correlate reasonably well to the metallic radius of the solute atom, although the as-milled $Fe_3As$ did contain a significant amount of intermetallic second phase. The 15% rule seems reasonably successful for the alloys in the present study prepared by ball milling, although here we are considering a much larger solubility, 25%, than the 5% that is typically used to define good solubility. We could try to translate this enhanced concentration range into a prediction of a larger atomic radius difference for 5% solubility as follows. If the enthalpy depends on concentration $c$ as $c(1-c)$, a solid solution with $c=0.25$ will have 4× the enthalpy as a solid solution with $c=0.05$. Assuming the Hume-Rothery size rule originates with an elastic energy that scales as the square of the atomic radius, we might expect that milling in a Spex mill will allow solubility to $c=0.05$ to be achieved for a radius difference of 30%. The problem is more complicated than this, however, since the configurational entropy of mixing helps stabilize the alloy of $c=0.25$, so the maximum radius difference should be less than 30%. We must also consider the nucleation of equilibrium intermetallic compounds during mechanical alloying, so a complete size factor rule will require more investigation.

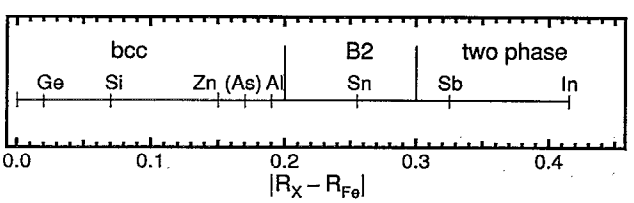


FIG. 6. Difference between the metallic radius of Fe and the radii of the solutes used in the present study, with approximate boundaries of the as-milled phases.

The second Hume-Rothery rule states that for good solubility, the electronegativity difference between the two elements should not be too large, typically within a range of ±0.4. This second rule was combined with the first rule by Darken and Gurry[23,24] in constructions such as that of Fig. 7. Figure 7 is a parametric plot of the Pauling electronegativity[43] versus the metallic radius.[21,42] The ellipse on the plot, centered about Fe, spans a horizontal range in metallic radius of ±15%, and a vertical range in electronegativity of ±0.4. (For the present plot, we scaled the axes so that the ellipse became a circle.) In the present study we found that all $Fe_3X$ alloys containing solutes inside the ellipse were bcc solid solutions after milling. Alloys of Al and As are near the edge of the ellipse, but $Fe_3Al$ was a bcc solid solution after milling, whereas $Fe_3As$ included a significant amount of $B8$ phase. It is interesting that both the electronegativity axis and the size axis of the ellipse, which are useful for predicting 5% thermodynamic solubility, are reasonable axes for predicting 25% solubility in alloys prepared with a Spex mill.

The small crystallite sizes of the alloys (Table I), could promote a grain-boundary segregation of solute atoms. Our x-ray diffractometry measurements were not sensitive to such grain-boundary segregations, but the $^{57}Fe$ Mössbauer spectra are sensitive to changes in local solute concentrations in the bcc phase. The problem is how to obtain an accurate

solute concentration in the bcc phase from the measured $^{57}$Fe HMF distributions. Such interpretations are well established for the solutes Al, Ge, and Si.[38] There was no indication of any strong loss of these solutes from the bcc phase, although the loss of a few percent is certainly possible. The analysis of $Fe_3Sn$, as shown in Fig. 4, was also successfully accomplished by assuming a solute concentration of 25%. The HMF distribution of $Fe_3Zn$ certainly did show a loss of Zn from the neighborhoods of $^{57}$Fe atoms, and this could be caused by the segregation of Zn atoms to grain boundaries (or a segregation of Zn atoms within the bcc grains). The Mössbauer spectra from the two-phase alloys $Fe_3As$ and $Fe_3Sb$ were less easy to interpret, but the narrowness of their HMF distributions at high fields implies some solute loss from the bcc phase. This implies a chemical heterogeneity in these alloys, which in turn could be related to the formation of the $B8$ intermetallic phase.

### B. Transient ordered phases

The $B2$ structure was found in as-milled $Fe_3Sn$. We suspect that the bcc phases in $Fe_3As$ and $Fe_3Sb$ also have partial $B2$ order, but interpretations of the x-ray and Mössbauer data were impaired by the contributions from the $B8$ phase in these alloys. The $B2$ structure comprises two interpenetrating simple cubic lattices, which provide for good packing of large and small atoms. Although the $B2$ structure is not an equilibrium phase for Fe-Sn, the large size difference between Fe and Sn atoms may promote $B2$ order in as-milled $Fe_3Sn$. We suggest that the lower symmetry equilibrium $B8_2$ and $B35$ phases of Fe-Sn develop a high defect enthalpy during milling, and are destabilized with respect to the higher symmetry $B2$ structure. We note that the $B2$ structure is an equilibrium high-temperature phase for $Fe_3Al$ and $Fe_3Si$, although ball milling disorders these alloys into the bcc phase.

When the as-milled $Fe_3Sn$ powder is annealed at 300 °C, there is the eventual formation of a two-phase microstructure of bcc $\alpha$-Fe plus hexagonal $B35$ FeSn. In the early stages of thermal annealing, however, the imperfect $B2$ structure of the as-milled powder becomes more ordered, eventually achieving nearly perfect order for the $Fe_3Sn$ stoichiometry. This transient ordering may occur for the same reasons that have been discussed theoretically.[13–18] The growth of $B2$ order should allow for some free-energy reduction in the alloy. The formation of equilibrium phases would reduce the free energy by an even greater amount, but this requires many more atom movements to form critical nuclei and allow them to grow. It may be kinetically expedient, therefore, for the alloy to develop a transient state of $B2$ order before the equilibrium phases are formed. The same argument applies to the formation of transient $D0_3$ order in $Fe_3Ge$. The $D0_3$ structure in $Fe_3Ge$ was more stable against the formation of equilibrium phases than was the $B2$ structure in $Fe_3Sn$. We note that the distance on the Darken–Gurry plot (Fig. 7) between Fe and Sn is larger than the distance between Fe and Ge. Perhaps there is a tendency of transient phases to be more long lived when this distance is not so large.

## V. CONCLUSION

We used mechanical alloying to prepare several alloys of the $Fe_3X$ composition, where the solutes, $X$=Al, As, Ge, In, Sb, Si, Sn, Zn, were all from groups IIB, IIIB, IVB, and VB of the periodic table. The trends in the as-milled phases largely followed the metallic radius of the solute atoms; for solutes with metallic radii increasingly different from that of Fe, a bcc solid solution (Ge, Si, Al, Zn) gives away to $B2$ order of the bcc Fe alloy (Sn) plus some intermetallic compound formation (As, Sb), and finally no bcc-based Fe alloy was observed for the largest solute (In). Even better predictions of bcc solid solubility were obtained with a modified Darken–Gurry plot of electronegativity versus metallic radius. The Hume-Rothery rules for 5% solubility in equilibrium alloys seem to translate to a 25% solubility for powders prepared by mechanical alloying.

Thermal stabilities of the as-milled bcc $Fe_3Ge$ and $B2$ $Fe_3Sn$ were tested. Transient $D0_3$ order in $Fe_3Ge$ and transient $B2$ order in $Fe_3Sn$ evolved before the nucleation of equilibrium intermetallics. The transient $D0_3$ order in $Fe_3Ge$ was much more stable than the transient $B2$ order in $Fe_3Sn$, however, possibly because the metallic radius difference of Fe and Ge is not so large as the difference between Fe and Sn.

## ACKNOWLEDGMENTS

We acknowledge stimulating conversations with L. Anthony. This work was supported by the U. S. Department of Energy under Contract No. DE-FG03-86ER45270.

[1] C. C. Koch and M. S. Kim, J. Phys. Paris C **8**, 573 (1985).
[2] E. Hellstern, L. Schultz, R. Bormann, and D. Lee, Appl. Phys. Lett. **53**, 1399 (1988).
[3] C. C. Koch, Ann. Rev. Mater. Sci. **19**, 121 (1989).
[4] E. Hellstern, H. J. Fecht, Z. Fu, and W. L. Johnson, J. Mater. Res. **4**, 1292 (1989).
[5] H. J. Fecht, E. Hellstern, Z. Fu, and W. L. Johnson, Adv. Powder Metall. **1–2**, 111 (1989).
[6] B. Fultz, G. LeCaër, and P. Matteazzi, J. Mater. Res. **4**, 1450 (1989).
[7] A. Calka and A. P. Radlinski, Scr. Metall. **23**, 1497 (1989).
[8] C. Suryanarayana and F. Froes, J. Mater. Res. **5**, 1880 (1990).
[9] C. Suryanarayana and R. Sundaresan, Mater. Sci. Eng. A **131**, 237 (1991).
[10] K. Uenishi, K. F. Kobayashi, K. N. Ishihara, and P. H. Shingu, Mater. Sci. Eng. A **134**, 1342 (1991).
[11] M. V. Zdujic, K. F. Kobayashi, and P. H. Shingu, J. Mater. Sci. **26**, 5502 (1991).
[12] D. K. Mukhopadhyay, C. Suryanarayana, and F. H. Froes, Scr. Metall. Mater. **30**, 133 (1994).
[13] L. Anthony and B. Fultz, J. Mater. Res. **4**, 1132 (1989).
[14] B. Fultz, Philos. Mag. B **67**, 253 (1993).
[15] L. Anthony and B. Fultz, J. Mater. Res. **9**, 348 (1994).
[16] W. A. Soffa and D. E. Laughlin, Acta Metall. **37**, 3019 (1989).
[17] L.-Q. Chen and A. G. Khachaturyan, Phys. Rev. B **44**, 4681 (1991).
[18] L. Reinhard and P. E. A. Turchi, Phys. Rev. Lett. **72**, 121 (1994).
[19] Z. Q. Gao and B. Fultz, Philos. Mag. B **67**, 787 (1993).
[20] Z. Gao and B. Fultz, Nanostruct. Mater. **2**, 231 (1993).
[21] W. Hume-Rothery and G. V. Raynor, *The Structure of Metals and Alloys* (Institute of Metals, London, 1962).
[22] A. Cottrell, *Introduction to the Theory of Metals* (Institute of Metals, London, 1988).
[23] K. A. Geschneider, Jr., in *Theory of Alloy Phase Formation*, edited by L. H. Bennett (TMS, Warrendale, PA, 1980), p. 1.
[24] L. S. Darken and R. W. Gurry, *Physical Chemistry of Metals* (McGraw-Hill, New York, 1953), p. 74.

[25] G. Le Caer and J. M. Dubois, J. Phys. E **12**, 1083 (1979).
[26] A. Laggoun, A. Hauet, and J. Teillet, Hyperfine Interact. **54**, 825 (1990).
[27] A. Hauet, A. Laggoun, and J. Teillet, Mater. Sci. Eng. A **148**, 123 (1991).
[28] H. P. Klug and L. E. Alexander, *X-Ray Diffraction Procedures* (Wiley-Interscience, New York, 1974), p. 594.
[29] H. P. Klug and L. E. Alexander, *ibid.*, p. 664.
[30] C. L. Chien, G. Xiao, and K. M. Unruh, Phys. Rev. B **32**, 5582 (1985).
[31] G. Xiao and C. L. Chien, Hyperfine Interact. **27**, 377 (1986).
[32] T. B. Massalski, *Binary Alloy Phase Diagrams* (ASM, Metals Park, OH, 1986).
[33] S. Nasu, S. Imaoka, S. Morimoto, H. Tanimoto, B. Huang, T. Tanaka, J. Kuyama, K. N. Ishihara, and P. H. Shingu, Mater. Sci. Forum **88–90**, 569 (1992).
[34] V. K. Singh, M. Singh, and S. Bhan, Phys. Status Solidi **74**, K115 (1982).
[35] M. Asanama, J. Phys. Soc. Jpn. **17**, 300 (1962).
[36] H. M. Rietveld, Acta Cryst . **20**, 508 (1966).
[37] B. Fultz, in *Mössbauer Spectroscopy Applied to Magnetism and Materials Science*, edited by G. J. Long and Fernande Grandjean (Plenum, New York, 1993), Vol. I, Chap. 1, pp. 1–31.
[38] B. Fultz, Z.-Q. Gao, H. H. Hamdeh, and S. A. Oliver, Phys. Rev. B **49**, 6312 (1994).
[39] H. Ouyang and B. Fultz, J. Appl. Phys. **66**, 4752 (1989).
[40] H. H. Hamdeh, S. A. Oliver, B. Fultz, and Z. Q. Gao, J. Appl. Phys. **74**, 5117 (1993).
[41] Z. Q. Gao, Ph.D. dissertation, Materials Science, California Institute of Technology, May 18, 1994.
[42] F. S. Galasso, *Structure and Properties of Inorganic Solids* (Pergamon, Oxford, England, 1970), pp. 8–11.
[43] Sargent–Welch Scientific Company, Skokie, 1980 compilation.